



HAL
open science

Acoustoelasticity in transversely isotropic soft tissues: Quantification of muscle nonlinear elasticity

Marion Bied, Jean-Luc Gennisson

► **To cite this version:**

Marion Bied, Jean-Luc Gennisson. Acoustoelasticity in transversely isotropic soft tissues: Quantification of muscle nonlinear elasticity. *Journal of the Acoustical Society of America*, 2021, 150 (6), pp.4489-4500. 10.1121/10.0008976 . hal-03856997

HAL Id: hal-03856997

<https://hal.science/hal-03856997>

Submitted on 17 Nov 2022

HAL is a multi-disciplinary open access archive for the deposit and dissemination of scientific research documents, whether they are published or not. The documents may come from teaching and research institutions in France or abroad, or from public or private research centers.

L'archive ouverte pluridisciplinaire **HAL**, est destinée au dépôt et à la diffusion de documents scientifiques de niveau recherche, publiés ou non, émanant des établissements d'enseignement et de recherche français ou étrangers, des laboratoires publics ou privés.

Acoustoelasticity in transversely isotropic soft tissues: Quantification of muscle nonlinear elasticity

Marion Bied and Jean-Luc Gennisson

Citation: [The Journal of the Acoustical Society of America](#) **150**, 4489 (2021); doi: 10.1121/10.0008976

View online: <https://doi.org/10.1121/10.0008976>

View Table of Contents: <https://asa.scitation.org/toc/jas/150/6>

Published by the [Acoustical Society of America](#)

ARTICLES YOU MAY BE INTERESTED IN

[Validation of cepstral peak prominence in assessing early voice changes of Parkinson's disease: Effect of speaking task and ambient noise](#)

[The Journal of the Acoustical Society of America](#) **150**, 4522 (2021); <https://doi.org/10.1121/10.0009063>

[Investigating urban soundscapes of the COVID-19 lockdown: A predictive soundscape modeling approach](#)

[The Journal of the Acoustical Society of America](#) **150**, 4474 (2021); <https://doi.org/10.1121/10.0008928>

[A numerical study of the coupling between Rayleigh streaming and heat transfer at high acoustic level](#)

[The Journal of the Acoustical Society of America](#) **150**, 4501 (2021); <https://doi.org/10.1121/10.0009026>

[Contribution of laryngeal size to differences between male and female voice production](#)

[The Journal of the Acoustical Society of America](#) **150**, 4511 (2021); <https://doi.org/10.1121/10.0009033>

[Acoustofluidic-mediated molecular delivery to human T cells with a three-dimensional-printed flow chamber](#)

[The Journal of the Acoustical Society of America](#) **150**, 4534 (2021); <https://doi.org/10.1121/10.0009054>

[The contrast between clear and plain speaking style for Mandarin tones](#)

[The Journal of the Acoustical Society of America](#) **150**, 4464 (2021); <https://doi.org/10.1121/10.0009142>



**Advance your science and career
as a member of the**

ACOUSTICAL SOCIETY OF AMERICA

LEARN MORE



Acoustoelasticity in transversely isotropic soft tissues: Quantification of muscle nonlinear elasticity

Marion Bied and Jean-Luc Gennisson^{a)}

BioMaps, Laboratoire d'Imagerie Biomédicale Multimodale à Paris-Saclay, Université Paris-Saclay, CEA, CNRS UMR 9011, INSERM UMR 1281, 4 Place du général Leclerc, 91401, Orsay, France

ABSTRACT:

Recent developments in the field of elastography aim at developing the quantification of new mechanical properties of tissues, that are complementary to the shear modulus, which is characteristic of the linear elastic properties of a quasi-incompressible medium. In this context, measurement of the elastic nonlinearity of tissues was recently proposed based on acoustoelasticity. Up to now, most of the experimental applications of acoustoelasticity theory using Landau formalism in human tissues have assumed isotropy. However, this strong hypothesis does not hold in all human tissues, such as muscles that are generally considered as transversely isotropic (TI). In this work, after reviewing the constraints imposed by TI symmetry on the linear and nonlinear elastic properties of TI media, the acoustoelasticity theory in TI incompressible media is developed and implemented experimentally on a TI polyvinyl alcohol phantom and on *ex vivo* muscular tissues. Based on this theory and on the evolutions of the shear wave speed, with respect to uniaxial static stress, the nonlinear elastic parameter A is experimentally quantified. The estimations of A in *ex vivo* bovine and porcine muscles are on the order of hundreds of kPa. This work paves the way for more thorough muscle mechanical properties characterization as well as for the development of a potential new biomarker. © 2021 Acoustical Society of America. <https://doi.org/10.1121/10.0008976>

(Received 30 April 2021; revised 17 November 2021; accepted 19 November 2021; published online 28 December 2021)

[Editor: James F. Lynch]

Pages: 4489–4500

I. INTRODUCTION

In the field of biomedical imaging, elastography aims at measuring mechanical properties of tissues to provide physicians with a quantifiable, reproducible, and precise alternative to palpation. By using ultrasound imaging, shear wave elastography (SWE) consists in deducing tissues' mechanical properties from the characteristics of shear wave propagation. Among the different techniques available, supersonic shear imaging (SSI) produces a conical shear wave in a supersonic regime based on the acoustic radiation force, by focusing ultrasound waves at successive depths (Bercoff *et al.*, 2004). SSI benefits from ultrasound ultrafast imaging to image the propagation of the generated shear wave. From this propagation movie, the shear wave speed v_s in the tissue is deduced and used to estimate the second order linear shear modulus (μ) of the tissues, based on the assumptions of tissues as linear, elastic, homogeneous, and isotropic media.

However, the linear stress–strain relation assumption is a simplifying hypothesis as tissues exhibit a nonlinear mechanical behavior, in part because of the finite extensibility of macromolecules composing tissues (Rosen and Jiang, 2019). For a more thorough mechanical characterization of tissues and for the development of new biomarkers, Gennisson *et al.* (2007) developed a measure of the 3rd order elastic nonlinear shear modulus (NLSM) of tissues,

which appears in the expression of the strain energy, using the invariants of the Green–Cauchy strain tensor (Landau *et al.*, 1985).

NLSM can be quantified by using the acoustoelasticity (AE) theory that was first established by Brillouin (1925) and further developed by Hugues and Kelly (1953) and Hayes and Rivlin (1961) in compressible and incompressible solids, respectively. Gennisson *et al.* (2007) then adapted the theory for quasi-incompressible soft solids with the aim of applying it on soft tissues. The AE theory consists in measuring the speed of shear waves in media under uniaxial stress and in deducing the NLSM from the variations of shear wave speeds with respect to the applied uniaxial stress. Bernal *et al.* (2016) combined SSI and static elastography to quantify locally the shear wave speed and the local stress to map the local NLSM, in *in vivo* breast lesions. This study proved the NL elastic modulus to be a potential new interesting biomarker available for physicians.

However, the AE theory, as it is derived by Gennisson *et al.* (2007), relies on the strong assumption of tissue isotropy. This hypothesis does not hold in all biological tissues, as in muscles. Indeed, such organs are composed of elongated thin cells (muscular fibers or myocytes) that are aligned in one specific direction. In the plane perpendicular to this direction, cells are more or less arranged randomly. Muscles can therefore be considered as a transverse isotropic (TI) medium.

TI media require a more complex characterization of their elastic properties to consider the specificities of their

^{a)}Electronic mail: jean-luc.gennisson@universite-paris-saclay.fr, ORCID: 0000-0001-8318-8237.

geometry. For example, the linear elastic behavior of incompressible TI media is fully described by the specification of three independent parameters (the shear moduli along and across the principal axis, respectively $\mu_{//}$ and μ_{\perp} , and the Young modulus along the fibers, $E_{//}$) (Chadwick, 1993; Spencer, 1984), while isotropic incompressible media are characterized by one single linear elastic modulus. Besides, at the first nonlinear order, there are four 3rd-order constants for incompressible TI media, as opposed to only one in incompressible isotropic media (Destrade *et al.*, 2010). Therefore, to characterize the elastic NL of TI quasi-incompressible media, such as muscles, the AE theory must be first revisited to include the TI geometry hypothesis.

In this paper, the AE theory is first developed for TI incompressible media to retrieve the expression of shear wave speed as a function of uniaxial stress. Based on these equations, a method for quantification of one of the 3rd order shear moduli of TI incompressible media is proposed. The latter is then implemented on a TI polyvinyl alcohol cryogel (PVA) phantom and on *ex vivo* bovine and porcine muscular tissues. To that end, the experimental setup and data processing are described, prior to presentation and discussion of estimations of TI nonlinear elasticity in biological tissues.

II. THEORETICAL BACKGROUND

In this section, a transversely isotropic (TI) incompressible material is considered. TI media are characterized by an infinite order rotation symmetry axis defining their principal axis. A plane perpendicular to this axis is therefore isotropic. To identify particle positions in the material, a Cartesian coordinate system (x_1, x_2, x_3) with the x_3 direction coinciding with the principal axis of the TI material is used. Finally, we recall that the linear elastic behavior of an incompressible TI material is fully described by three independent elastic moduli (Chadwick, 1993; Spencer, 1984; Bower, 2010): $\mu_{//}$, μ_{\perp} (the shear moduli parallel and perpendicular to the principal axis, respectively), and $E_{//}$ (the Young modulus parallel to the principal axis).

The AE theory derived here for TI incompressible lossless media is highly inspired from the AE theory in isotropic media of Genisson *et al.* (2007). The aim of the following development is to express the speed of shear waves in the considered medium under uniaxial stress. Note that it recovers the results of Destrade *et al.* (2010), who used a different approach, based on the equations of incremental elasticity.

A. Overall governing equations for the retrieval of the motion equation of particles

Acoustic wave equations can be derived from the equation of motion of the medium's particles (given by Newton's second law), which is expressed in terms of Lagrangian coordinates \vec{a} (i.e., the particles' equilibrium

positions) as (Einstein's summation convention of repeated indices is used)

$$\rho_0 \ddot{u}_i = \frac{\partial P_{ik}}{\partial a_k}, \quad (1)$$

where ρ_0 is the medium's density, u_i the displacement of particles in the i direction, and P_{ik} is the components of the first Piola–Kirchhoff stress tensor. In the general case (without any incompressibility constraint), the latter is derived from the strain energy density e of the medium,

$$P_{ik} = \frac{\partial e}{\partial \left(\frac{\partial u_i}{\partial a_k} \right)}. \quad (2)$$

B. Expression of the strain energy density of TI incompressible media

Developed up to the 3rd order in terms of the Green–Lagrange strain tensor ε , the strain energy e of a compressible TI medium for which the principal direction is along \vec{x}_p , is (Johnson, 1982; Spencer, 1984)

$$\begin{aligned} e = & \frac{\lambda}{2} I_1^2 + \mu_{\perp} I_2 + \alpha I_1 I_4 + \frac{\beta}{2} I_4^2 + 2(\mu_{//} - \mu_{\perp}) I_5 \\ & + \frac{A}{3} I_3 + B I_1 I_2 + C I_1^3 + D I_1^2 I_4 \\ & + E I_1 I_4^2 + F I_1 I_5 + G I_4^3 + H I_4 I_5 + J I_2 I_4, \end{aligned} \quad (3)$$

where $\varepsilon_{ij} = \frac{1}{2} (\partial u_i / \partial a_j + \partial u_j / \partial a_i + (\partial u_i / \partial a_i)(\partial u_j / \partial a_j))$. $I_1 = \text{Tr}(\varepsilon)$, $I_2 = \text{Tr}(\varepsilon^2)$, and $I_3 = \text{Tr}(\varepsilon^3)$ are the invariants of ε defined by Landau and Lifshitz (1985). $I_4 = \vec{x}_p \cdot \varepsilon \cdot \vec{x}_p$ and $I_5 = \vec{x}_p \cdot \varepsilon^2 \cdot \vec{x}_p$ are the two additional ε invariants to consider in a TI medium and that are defined relative to the principal axis of the medium (note that for $\vec{x}_p = \vec{x}_3$, $I_4 = \varepsilon_{33}$ and $I_5 = \varepsilon_{13}^2 + \varepsilon_{23}^2 + \varepsilon_{33}^2$). λ , α , β , $\mu_{//}$ and μ_{\perp} are the five linear elastic coefficients of a TI medium defined by Spencer (1984) that appear naturally in the definition of the elastic tensor of the medium. Their relations with the engineering parameters for TI media (the two Young moduli, shear moduli, and Poisson ratios) appearing conventionally in the elastic compliance tensor are given elsewhere (Bower, 2010; Namani *et al.*, 2012). The nine 3rd order elastic parameters of a TI medium are $(A, B, C, D, E, F, G, H, J)$. Note that for convenience, these parameters are linear combinations of those originally used by Johnson (1982).

In TI incompressible media, there is no relative volume change, which translates into $III_C = \frac{\rho_0}{\rho} \rightarrow 1$, where III_C is the 3rd principal invariant of the Green deformation tensor. Due to the relation between III_C and the Green–Lagrange strain tensor invariants (Destrade *et al.*, 2010), this condition implies that I_1 is a second order term in terms of ε ,

$$I_1 = I_2 - \frac{4}{3} I_3 - I_1^2 + 2I_1 I_2 - \frac{2}{3} I_1^3. \quad (4)$$

Moreover, in terms of the linear elastic parameters, the incompressibility assumption yields $\lambda \rightarrow \infty$. Consequently, using the relations of correspondence between $(\lambda, \alpha, \beta, \mu_{//},$

μ_{\perp}) and the engineering parameters (Bower, 2010; Namani et al., 2012), β and $E_{//}$ are linked through the relation

$$E_{//} = \beta + 4\mu_{//} - \mu_{\perp}. \tag{5}$$

Therefore, after inserting Eqs. (4) and (5) in Eq. (3) and neglecting all fourth and upper order terms in ε , the strain energy e of a TI incompressible medium, for which the principal direction is \vec{x}_3 , is up to a constant

$$\begin{aligned} e = & \mu_{\perp} I_2 + \frac{E_{//} - 3\mu_{\perp}}{2} \varepsilon_{33}^2 + 2(\mu_{//} - \mu_{\perp})(\varepsilon_{13}^2 + \varepsilon_{23}^2) \\ & + \frac{A}{3} I_3 + (G + H + K) \varepsilon_{33}^3 + (H + 2K) \varepsilon_{33} (\varepsilon_{13}^2 + \varepsilon_{23}^2) \\ & + K \varepsilon_{33} (\varepsilon_{11}^2 + \varepsilon_{22}^2 + 2\varepsilon_{12}^2). \end{aligned} \tag{6}$$

In the previous equation, the invariant I_2 has been developed in terms of ε elements when appearing in the 3rd order strain terms, and the $K = J + \alpha$ modulus has been introduced. Note that in the incompressibility limit, λ tends toward infinity (Bower, 2010; Namani et al., 2012): without prior knowledge of the value of the 3rd order elastic modulus J, K can therefore potentially be infinite. This also raises the question of the implications of the latter remark for the finite nature of the strain energy. Similar to Hamilton et al. (2004) work in the isotropic case, further repackaging of the strain energy density for TI material in the incompressible limit based on comparisons between the Green–Lagrange strain terms and logarithmic strain considerations is needed to address the issue raised by the potential infinite nature of K. However, such a theoretical work is out of the scope of this article. Nevertheless, the strain energy expression [Eq. (6)] has already been used in previous works (Destrade et al., 2010; Remenieras et al., 2021: the K modulus corresponds to their α_3 modulus) that did not raise the issue. Moreover, the experimental quantities we report in the next sections, as well as those measured by Remenieras et al. (2021), are finite, even though they theoretically involve the K (or α_3) modulus. Despite this remark, the expression of the strain energy in Eq. (6) is used as the starting point of the AE theory developed hereafter in Sec. IIC.

C. Equation of motion of particles of a TI incompressible medium in the context of AE SWE experiments

After injecting the expression of the strain energy of TI incompressible media [Eq. (6)] in Eq. (2), the first Piola–Kirchhoff stress tensor is obtained. Note that compared to previous works (Ogden, 1984; Chadwick, 1993), the first Piola–Kirchhoff stress tensor should include a supplementary Lagrange multiplier term to ensure the incompressibility constraint. Indeed, as demonstrated by Chadwick (1993), the first Piola–Kirchhoff stress tensor expression obtained from Eq. (2) in a compressible TI medium includes an additional term involving the $\kappa \text{Tr}(\varepsilon)$ product where κ is the bulk modulus. However, in the incompressible limit, κ tends to infinity and $\text{Tr}(\varepsilon)$ towards zero. Therefore, to remove the ambiguity of the $\kappa \text{Tr}(\varepsilon)$ limit, a Lagrange multiplier is

introduced and results in an additional pressure term in the first Piola–Kirchhoff tensor. The specific expression of this Lagrange multiplier term can be determined separately considering the boundary conditions [see Eq. (3.7) in Chadwick (1993) for details]. Here, beyond the consideration of the strain energy expression of TI incompressible media [Eq. (6)], the static displacement field created by the uniaxial external stress in an AE experiment is assumed to be isochoric [we refer the readers to Eq. (11)], which is consistent with the incompressibility hypothesis. Incompressibility is thus enforced at that point and the Lagrange multiplier term is therefore not considered at this stage.

Knowing the expression of the first Piola–Kirchhoff stress tensor, the equation of motion of particles is retrieved based on Eq. (1). In the context of AE experiments, different assumptions can be made to further simplify the equation of motion derived at this stage.

First, in an AE experiment, an acoustic wave propagates in a stressed medium. The displacement \vec{u} of any particle in the medium can therefore be decomposed into two components: a static term \vec{u}^S due to the uniaxial stress and a dynamic term \vec{u}^D induced by the propagation of the elastic wave. This implies: $\vec{u} = \vec{u}^S + \vec{u}^D$. When considering AE SWE experiments, the acoustic wave at hand is a shear wave generated by the acoustic radiation force (Bercoff et al., 2004). This implies that the dynamic displacement amplitude is micrometric, which is very small compared to the static displacement. Therefore, in the equation of motion, the non-linear propagation of the shear wave (i.e., product terms implying \vec{u}^D derivatives) can be neglected. Furthermore, higher order static deformations (i.e., second order derivatives in \vec{u}^S) will be neglected.

Second, shear waves generated in SSI are linearly polarized and studied in the imaging plane: the measured shear wave speed is therefore an estimation of that of linearly polarized plane shear waves. Therefore, the following development will be restricted to the case of linearly polarized plane shear waves. For a plane shear wave linearly polarized in the i direction, the dynamic displacement \vec{u}^D is reduced to its x_i component ($\vec{u}^D = u_i^D \vec{n}_i$, where \vec{n}_i is the unit vector in the i direction) and only depends on time and on a_p , the position along the propagation direction p of the wave ($\frac{\partial u_l^D}{\partial a_i} = 0$ for $l \neq p$). Furthermore, for simplification, the polarization and propagation directions of the shear waves are chosen to be either parallel or perpendicular to the principal direction of the TI medium (see Fig. 1 for definition of the considered configurations): thus, they coincide with two of the axes of the coordinate system (which includes one axis parallel to the principal direction of the TI medium). Finally, the medium is subjected to a uniaxial stress, implying that only longitudinal static strains are non-zero. Static displacements therefore verify: $\frac{\partial u_l^S}{\partial a_j} = 0$ for $l \neq j$.

The aforementioned approximations and simplifications yield the following equation of motion ($\delta_{m,n}$ is the Kronecker delta):

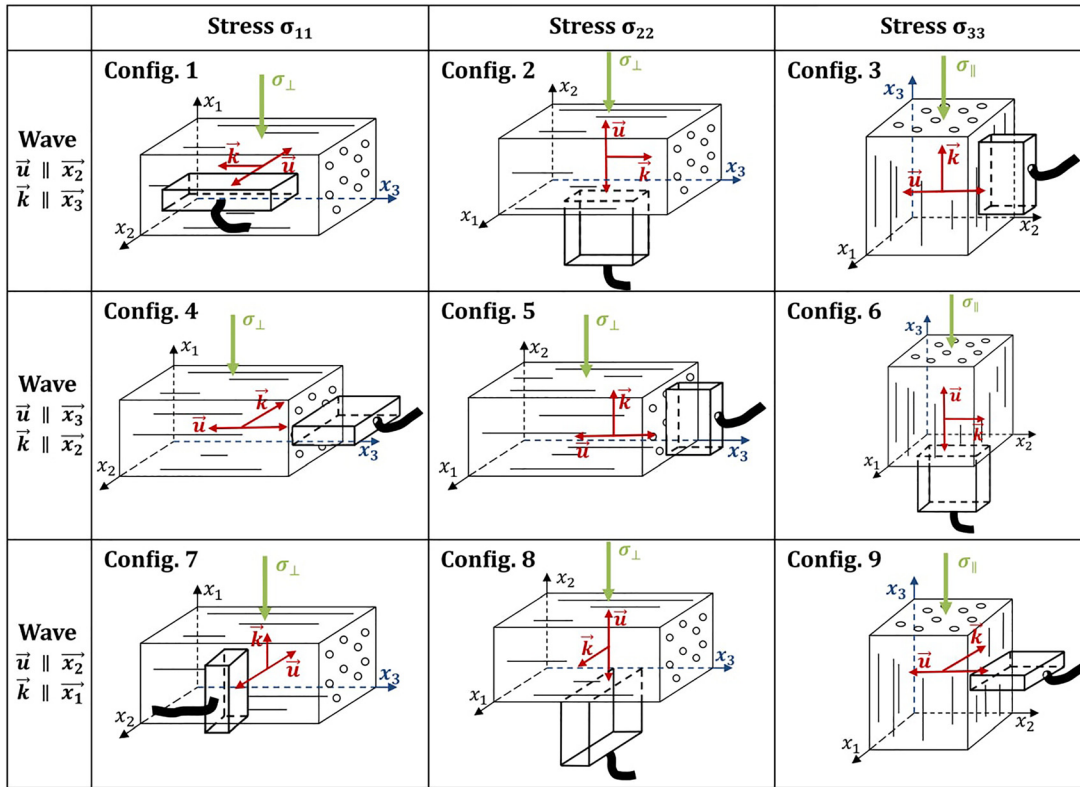


FIG. 1. (Color online) The 9 simplest configurations considered for the derivation of the AE theory in TI medium in this paper. The principal axis of the TI medium is chosen to be along x_3 (in blue). For each configuration, the directions of polarization \vec{u} and propagation \vec{k} of the shear wave are specified in red, as well as the orientation of the stress σ in green. In the framework of SSI (used for experimental validation and use of the theory), the positioning and orientation of the ultrasound probe are represented. The indicated configuration numbers are used to refer to each configuration throughout the article. Note that in the two first lines, due to TI symmetry, the x_2 and x_1 orientations can be interchanged. To get back to configurations equivalent to those defined in the figure, the stress orientations (along x_2 and x_1) must also be rotated.

$$\begin{aligned}
 \rho_0 \frac{\partial^2 u_i^D}{\partial t^2} = & \mu_{\perp} \frac{\partial^2 u_i^D}{\partial a_p^2} + 2 \left(\mu_{\perp} + \frac{A}{4} \right) \left(\frac{\partial u_i^S}{\partial a_i} \frac{\partial^2 u_i^D}{\partial a_p^2} + \frac{\partial u_p^S}{\partial a_p} \frac{\partial^2 u_i^D}{\partial a_p^2} \right) + (E_{\parallel} - 3\mu_{\perp}) \frac{\partial u_3^S}{\partial a_3} \frac{\partial^2 u_i^D}{\partial a_3^2} \\
 & + (\mu_{\parallel} - \mu_{\perp}) \left\{ \delta_{i,3} \left[\frac{\partial^2 u_3^D}{\partial a_1^2} + \frac{\partial^2 u_3^D}{\partial a_2^2} + 2 \frac{\partial u_3^S}{\partial a_3} \left(\frac{\partial^2 u_3^D}{\partial a_1^2} + \frac{\partial^2 u_3^D}{\partial a_2^2} \right) \right] + \delta_{i,1} \left(\frac{\partial^2 u_1^D}{\partial a_3^2} + 2 \frac{\partial u_1^S}{\partial a_1} \frac{\partial^2 u_1^D}{\partial a_3^2} \right) \right. \\
 & \left. + \delta_{i,2} \left(\frac{\partial^2 u_2^D}{\partial a_3^2} + 2 \frac{\partial u_2^S}{\partial a_2} \frac{\partial^2 u_2^D}{\partial a_3^2} \right) \right\} + \frac{H + 2K}{2} \left[\delta_{i,3} \frac{\partial u_3^S}{\partial a_3} \left(\frac{\partial^2 u_3^D}{\partial a_1^2} + \frac{\partial^2 u_3^D}{\partial a_2^2} \right) + \delta_{i,1} \frac{\partial u_3^S}{\partial a_3} \frac{\partial^2 u_1^D}{\partial a_3^2} + \delta_{i,2} \frac{\partial u_3^S}{\partial a_3} \frac{\partial^2 u_2^D}{\partial a_3^2} \right] \\
 & + K \left(\delta_{i,1} \frac{\partial u_3^S}{\partial a_3} \frac{\partial^2 u_1^D}{\partial a_2^2} + \delta_{i,2} \frac{\partial u_3^S}{\partial a_3} \frac{\partial^2 u_2^D}{\partial a_1^2} \right). \tag{7}
 \end{aligned}$$

D. Derivation of the NL elastodynamic equation in the configuration where wave polarization and stress are along x_2 , and wave propagation along x_3 (configuration 8)

Let us now consider, as in the experimental configurations represented in the 3rd line of Fig. 1, plane shear waves linearly polarized in the x_2 direction and propagating along the x_1 direction. For such configurations, the equation of motion [Eq. (7)] reduces to

$$\rho_0 \frac{\partial^2 u_2^D}{\partial t^2} = \frac{\partial^2 u_2^D}{\partial a_1^2} \left[\mu_{\perp} + 2 \left(\mu_{\perp} + \frac{A}{4} \right) \left(\frac{\partial u_1^S}{\partial a_1} + \frac{\partial u_2^S}{\partial a_2} \right) + K \frac{\partial u_3^S}{\partial a_3} \right]. \tag{8}$$

To go further and get the wave equation in a form, such that the wave velocity can be retrieved, the equation of motion must be expressed with respect to the current state (Eulerian) coordinates and not using that of the equilibrium state. In an AE experiment, three different states can be used

to refer to a particle: the equilibrium state \vec{a} , the initial state \vec{x} (i.e., the medium under stress: $\vec{x} = \vec{a} + u^S$) and the current state \vec{y} , which is related to the shear wave propagation ($\vec{y} = \vec{x} + u^D$) and corresponds to the Eulerian coordinates. Because of the infinitesimal amplitude of the shear wave, the initial and current states are considered to coincide $\vec{y} \approx \vec{x}$. Therefore, a change of variable from \vec{a} to \vec{x} (with $\vec{a} = \vec{x} - u^S$) must be undertaken in Eq. (8) to get the desired form of the wave equation. By use of the chain rule and by neglecting the nonlinear static displacement terms, this change of variables consists in applying the following approximations:

$$\frac{\partial u_k^S}{\partial a_k} \approx \frac{\partial u_k^S}{\partial x_k}, \quad \frac{\partial^2 u_i^D}{\partial a_k^2} \approx \frac{\partial^2 u_i^D}{\partial x_k^2} \left(1 + 2 \frac{\partial u_k^S}{\partial x_k} \right) \quad (9)$$

for $i, k = 1, 2$, or 3 .

This change of variable in the equation of motion expressed in Eq. (8) yields

$$\rho_0 \frac{\partial^2 u_2^D}{\partial t^2} = \frac{\partial^2 u_2^D}{\partial x_1^2} \left[\mu_{\perp} + \frac{\partial u_1^S}{\partial x_1} \left(4\mu_{\perp} + \frac{A}{2} \right) + \frac{\partial u_2^S}{\partial x_2} \left(2\mu_{\perp} + \frac{A}{2} \right) + K \frac{\partial u_3^S}{\partial x_3} \right]. \quad (10)$$

Since the uniaxial stress is small, NL static displacement terms can be neglected and Hooke's law in TI incompressible media (Bower, 2010; Namani et al., 2012) can therefore be used to express the static displacement derivatives as a function of the local stress. Let us consider a uniaxial stress along the \vec{x}_2 axis (case number 8 as defined in Fig. 1); then

the application of Hooke's law yields (σ_{22} is set positive but a compression is applied; hence, the negative sign for ε_{22})

$$\begin{aligned} \frac{\partial u_1^S}{\partial x_1} &\approx \varepsilon_{11} \approx \frac{\nu_{\perp}}{E_{\perp}} \sigma_{22}, & \frac{\partial u_2^S}{\partial x_2} &\approx \varepsilon_{22} \approx -\frac{1}{E_{\perp}} \sigma_{22}, \\ \frac{\partial u_3^S}{\partial x_3} &\approx \varepsilon_{33} \approx \frac{\nu_{31}}{E_{\parallel}} \sigma_{22} \end{aligned} \quad (11)$$

[with $\nu_{\perp} = \frac{E_{\parallel} - \mu_{\perp}}{E_{\parallel} + \mu_{\perp}}$, $E_{\perp} = \frac{4\mu_{\perp}}{E_{\parallel} + \mu_{\perp}} E_{\parallel}$ and $\nu_{31} = \frac{1}{2}$ for TI incompressible media (Namani et al., 2012)]. Note that these relations are valid only in the case of uniaxial stress and that σ_{22} refers to the local stress. However, if the applied stress is assumed to be uniform in the medium, σ_{22} corresponds to the external stress applied by the experimenter on the medium.

Replacing the static displacement derivatives in Eq. (10) by their expressions in Eq. (11) yields the following shear wave speed v_s relation for configuration 8:

$$\rho_0 v_s^2 = \mu_{\perp} + \frac{\sigma_{22}}{2E_{\parallel}} \left(E_{\parallel} - 3\mu_{\perp} - \frac{A}{2} + K \right). \quad (12)$$

The previous reasoning has been applied in the eight other configurations defined in Fig. 1, yielding the equations specified in Table I.

Note that at zero stress, the elastic linear behavior of the medium is recovered. In the case of incompressible isotropic media [which translates into $\mu_{//} = \mu_{\perp} = \mu_0$, $E_{//} = E_{\perp} = E = 3\mu_0$, and $H = K = 0$ (Johnson, 1982)], the equations obtained match those found by Gennisson et al. (2007) in the corresponding configurations.

TABLE I. Nonlinear elastodynamic equations in the simplest nine AE configurations for a TI incompressible medium. Refer to Fig. 1 and its legend for the definition of the configurations and variables \vec{u} , \vec{k} , and σ .

Shear wave	Stress axis	Configurations	Nonlinear elastodynamic equations
$\vec{u} \parallel \vec{x}_2$	σ_{11}	1	$\rho_0 v_s^2 = \mu_{\parallel} + \frac{\sigma}{2E_{\parallel}} \left[E_{\parallel} - \mu_{\perp} + \mu_{\parallel} + \frac{\mu_{\parallel} E_{\parallel}}{\mu_{\perp}} + \frac{A}{4} \left(1 + \frac{E_{\parallel}}{\mu_{\perp}} \right) + \frac{H + 2K}{2} \right]$
$\vec{k} \parallel \vec{x}_3$	σ_{22}	2	$\rho_0 v_s^2 = \mu_{\parallel} + \frac{\sigma}{2E_{\parallel}} \left[E_{\parallel} - \mu_{\perp} + \mu_{\parallel} - \frac{\mu_{\parallel} E_{\parallel}}{\mu_{\perp}} + \frac{A}{4} \left(1 - \frac{E_{\parallel}}{\mu_{\perp}} \right) + \frac{H + 2K}{2} \right]$
	σ_{33}	3	$\rho_0 v_s^2 = \mu_{\parallel} - \frac{\sigma}{E_{\parallel}} \left(E_{\parallel} - \mu_{\perp} + \mu_{\parallel} + \frac{A}{4} + \frac{H + 2K}{2} \right)$
$\vec{u} \parallel \vec{x}_3$	σ_{11}	4	$\rho_0 v_s^2 = \mu_{\parallel} + \frac{\sigma}{2E_{\parallel}} \left[E_{\parallel} - \mu_{\perp} + \mu_{\parallel} + \frac{\mu_{\parallel} E_{\parallel}}{\mu_{\perp}} + \frac{A}{4} \left(1 + \frac{E_{\parallel}}{\mu_{\perp}} \right) + \frac{H + 2K}{2} \right]$
$\vec{k} \parallel \vec{x}_2$	σ_{22}	5	$\rho_0 v_s^2 = \mu_{\parallel} + \frac{\sigma}{2E_{\parallel}} \left[-E_{\parallel} - \mu_{\perp} + \mu_{\parallel} - \frac{\mu_{\parallel} E_{\parallel}}{\mu_{\perp}} + \frac{A}{4} \left(1 - \frac{E_{\parallel}}{\mu_{\perp}} \right) + \frac{H + 2K}{2} \right]$
	σ_{33}	6	$\rho_0 v_s^2 = \mu_{\parallel} - \frac{\sigma}{E_{\parallel}} \left(-\mu_{\perp} + \mu_{\parallel} + \frac{A}{4} + \frac{H + 2K}{2} \right)$
$\vec{u} \parallel \vec{x}_2$	σ_{11}	7	$\rho_0 v_s^2 = \mu_{\perp} - \frac{\sigma}{2E_{\parallel}} \left(E_{\parallel} + 3\mu_{\perp} + \frac{A}{2} - K \right)$
$\vec{k} \parallel \vec{x}_1$	σ_{22}	8	$\rho_0 v_s^2 = \mu_{\perp} - \frac{\sigma}{2E_{\parallel}} \left(-E_{\parallel} + 3\mu_{\perp} + \frac{A}{2} - K \right)$
	σ_{33}	9	$\rho_0 v_s^2 = \mu_{\perp} + \frac{\sigma}{E_{\parallel}} \left(3\mu_{\perp} + \frac{A}{2} - K \right)$

E. Method for quantification of the nonlinear shear modulus A of incompressible transversely isotropic media

In all nine derived AE equations, there is an affine relationship between the apparent shear modulus of the stressed medium ($\mu = \rho_0 v_S^2$) and the applied stress (σ). Moreover, the equations are not independent from each other. Indeed, by naming γ_i the multiplying coefficient associated with the stress in configuration i (configuration numbers defined in Fig. 1), one finds (note that only non-equivalent relations are written)

$$\begin{aligned} \gamma_1 &= \gamma_4; \quad \gamma_2 - \gamma_5 = 1; \quad \gamma_3 - \gamma_6 = -1; \\ \gamma_7 - \gamma_8 &= -1; \quad \gamma_8 + \frac{\gamma_9}{2} = \frac{1}{2}; \quad \gamma_1 + \gamma_2 + \gamma_6 = 1. \end{aligned} \tag{13}$$

Configurations 1 and 4 are therefore strictly equivalent. Indeed, in both configurations, the shear deformations generated by the shear waves are in the same plane (defined by the polarization and propagation directions) with respect to the principal axis of the TI medium. Moreover, the stress is applied perpendicularly to the shear plane.

Based on Eq. (13) and on the expressions of γ_i in terms of the linear ($\mu_{//}, \mu_{\perp}, E_{//}$) and NL (A, H, K) shear moduli, A can be experimentally estimated using the measurements of γ_1 and γ_2 ,

$$A = 4\mu_{\perp} \left(\gamma_1 - \gamma_2 - \frac{\mu_{//}}{\mu_{\perp}} \right). \tag{14}$$

In Secs. III and IV, the SSI technique will be used to assess the evolution of the shear wave speed with respect to stress in a TI PVA phantom and in *ex vivo* muscles, with the aim of validating the AE theory developed previously and providing the first estimations of A , one of the NLSM of TI incompressible media.

III. MATERIAL AND METHODS

A. Transverse isotropic samples

AE experiments were carried on a TI phantom and on *ex vivo* muscular tissues.

1. Transverse isotropic polyvinyl alcohol phantom

TI polyvinyl alcohol (PVA) phantoms were produced based on previous work by Chatelin *et al.* (2014). PVA (Polyvinyl alcohol hydrolyzed, Sigma-Aldrich, St. Louis, MO) (10% in mass) was dissolved in 95 °C heated water. Sigmacell (Sigmacell Cellulose type 20, Sigma-Aldrich, St. Louis, MO) (1% in mass) was added as scatterers in the cooled solution (at room temperature). The mixture was then poured in a parallelepipedal mould for three successive isotropic freezing–thawing cycles (15 h at –18 °C for freezing, 9 h at 25 °C immersed in water for thawing). Anisotropy was generated during the next 3 freezing–thawing cycles, during which the phantom was removed from the mould, placed in a jaw system, and stretched in the jaw direction to its maximum [Fig. 2(A)]. Stretching during these freezing–thawing cycles causes PVA to polymerize in the stretching direction, which defines therefore, the principal direction of the resulting TI PVA phantom. The phantom was cut to preserve only the parts undamaged by the jaw system: its final dimensions were 6.0 × 7.0 × 5.0 cm³. The phantom was stored at room temperature in water.

2. Biological transverse isotropic soft tissues

Beef and pork tenderloins with the most visible and aligned muscular fibers were chosen at the butcher on the morning of the experiments. They were then carefully cut to obtain a parallelepipedal sample with the long edges parallel to the muscular fibers. This way, the two faces perpendicular to the long edges correspond to isotropic planes of the TI medium. The *ex vivo* muscular tissues were typically

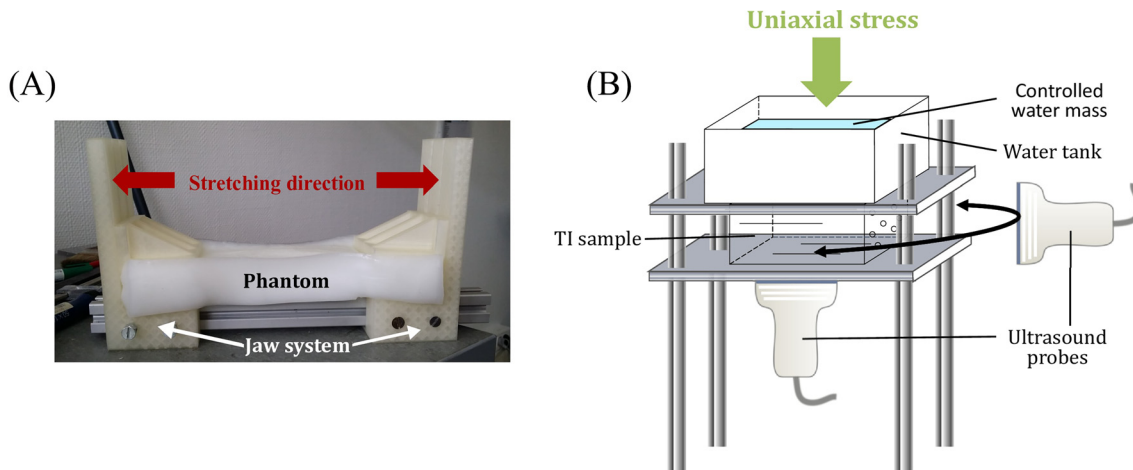


FIG. 2. (Color online) Experimental setups for TI phantom construction and AE experiments. (A) Picture of the jaw system allowing the stretching of the PVA phantom during the anisotropic freezing–thawing cycles for anisotropy generation in the phantom. (B) Diagram of the experimental setup used for AE experiments. By filling the water tank with a known water mass, a controlled uniaxial stress is generated. Ultrasound probes are placed at the bottom or on the side of the sample and oriented relatively to the principal direction of the TI sample to match any of the nine configurations defined in Fig. 1.

5.0–6.0 cm thick. Their surface ranged from $7.0 \times 7.0 \text{ cm}^2$ to $13.0 \times 11.5 \text{ cm}^2$ (the precise dimensions of the samples are specified in Table II). These samples were assumed to be homogenous and TI.

B. Experimental setup

1. Uniaxial stress

The experimental setup designed to carry out the AE experiments is highly inspired from Gennisson *et al.* (2007) and is represented in Fig. 2(B). Briefly, the sample lies in between two plexiglass plates. To generate uniaxial (vertical) stresses, a water tank covering the entire surface of the sample is positioned on top of the upper plate. Stresses of various and known amplitudes are applied by filling the tank with water incrementally by 0.1 or 0.2 kg steps up to 10–12 times, depending on the sample’s hardness and on the stability of the system. The contact surface S between the sample and the top plexiglass plate is measured to compute the amplitude of the stress σ : $\sigma = \frac{mg}{S}$ (with m the total mass on top of the sample, $g = 9.81 \text{ m} \cdot \text{s}^{-2}$ the standard gravity). Up to 2 kPa stresses were obtained. The plates are covered with coupling gel to minimize friction with the sample. This way, the generated stresses are assumed to be applied homogeneously in the whole sample: in such conditions, the local stress in the sample is considered equal to the applied external stress. Besides, the strains resulting from stresses applied using this setup are considered linear with stress, as suggested by Latorre-Ossa *et al.* (2012) work, in which they validated such an assumption by comparing simulations and experimental results.

2. Measurement of the shear wave group velocity

Two ultrasound probes [SL-10-2 (6 MHz central frequency) or SLH-20-6 (12 MHz central frequency), SuperSonic Imaging, Aix-en-Provence, France] were connected to an ultrafast ultrasound scanning device Aixplorer V12 (SuperSonic Imagine,



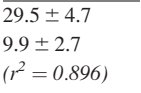







Aix-en-Provence, France), set on the musculo-skeletal preset. The shear wave group velocity is measured using the elastography mode of the scanner, based on the SSI technique (Bercoff *et al.*, 2004). The focusing of ultrasounds at four successive depths creates an ultrasonic radiation force, generating a quasi-cylindrical shear wave for which polarization is aligned with the probe axis. The central frequency of this generated broadband shear wave is around 250 Hz: hence, its wavelength is on the order of the centimeter. Given the larger size of the samples, shear body waves are considered to be at hand. Moreover, no dispersion effects *ex vivo*, are observed in accordance with literature (Gennisson *et al.*, 2010). The propagation of the wave in the imaging plane is imaged at an 8 kHz frame rate using ultrafast ultrasound imaging. In post-processing, the axial displacements due to the shear wave are quantified by correlating each frame with the next one and thanks to a time-of-flight algorithm, the local shear wave speed is retrieved. This sequence is repeated four times at four different lateral positions to cover the whole field of view. The local shear wave speed map is obtained and exported for processing using the AE theory.

The two probes were placed in contact with the sample [Fig. 2(B)]: either below the sample thanks to a SL-10-2 (SL 10-2, SuperSonic Imagine, Aix-en-Provence, France) probe mold embedded in the bottom plexiglass plate, or on the side of the sample, vertically or horizontally depending on the measured configuration. Since SLH-20-6 (SLH 20-6, SuperSonic Imagine, Aix-en-Provence, France) probes are half as long as SL-10-2 probes, the former were used in the vertical configurations to cope with the limited thickness of the sample. The probes were oriented as desired with respect to the principal axis of the medium which was detected beforehand by eye.

C. Data analysis based on the AE theory

For each AE measurement series (i.e., a set of shear wave speed maps corresponding to one configuration and

TABLE II. Experimental AE data obtained for each configuration and investigated sample. The surface of each sample, necessary for the computation of the stress, is specified. For each configuration, the linear shear modulus μ_{\parallel} or μ_{\perp} (depending on the configuration at hand) and the slope of the apparent shear modulus-stress relation are reported. The R-squared values associated with each linear regression are also specified.

Sample		TI-PVA	Beef muscle (1)	Beef muscle (2)	Pork muscle (3)	Pork muscle (4)
Surface of the sample (length x width in cm)		6.0 x 7.0	13.0 x 11.5	7.0 x 7.0	8.0 x 10.0	6.0 x 9.0
Config. 1	μ_{\parallel} (kPa)	29.4 ± 2.1	58.8 ± 15.6	53.2 ± 1.5	38.7 ± 2.7	21.1 ± 6.2
	γ_1	3.0 ± 0.4 ($r^2 = 0.979$)	15.0 ± 5.6 ($r^2 = 0.783$)	27.1 ± 7.4 ($r^2 = 0.886$)	7.1 ± 3.9 ($r^2 = 0.867$)	18.4 ± 3.7 ($r^2 = 0.933$)
Config. 2	μ_{\parallel} (kPa)	30.4 ± 2.0	54.4 ± 10.5	55.4 ± 2.3	45.3 ± 6.5	25.3 ± 4.6
	γ_2	-4.7 ± 1.8 ($r^2 = 0.873$)	19.5 ± 1.9 ($r^2 = 0.981$)	15.4 ± 1.9 ($r^2 = 0.968$)	4.0 ± 2.4 ($r^2 = 0.786$)	12.0 ± 4.2 ($r^2 = 0.843$)
Config. 4	μ_{\parallel} (kPa)	28.6 ± 2.1			34.5 ± 4.5	25.1 ± 2.5
	γ_4	2.4 ± 0.7 ($r^2 = 0.881$)			9.0 ± 4.4 ($r^2 = 0.769$)	22.0 ± 6.9 ($r^2 = 0.872$)
Config. 7	μ_{\perp} (kPa)		29.5 ± 4.7		22.7 ± 4.8	17.2 ± 2.3
	γ_7		9.9 ± 2.7 ($r^2 = 0.896$)		15.9 ± 3.3 ($r^2 = 0.948$)	8.7 ± 3.1 ($r^2 = 0.938$)
Config. 8	μ_{\perp} (kPa)	13.3 ± 0.7	23.7 ± 4.5	19.0 ± 2.4		21.4 ± 3.5
	γ_8	1.0 ± 0.3 ($r^2 = 0.824$)	10.0 ± 2.0 ($r^2 = 0.942$)	6.0 ± 1.0 ($r^2 = 0.965$)		8.0 ± 1.9 ($r^2 = 0.909$)

obtained on one sample, under different stresses), a region of interest (ROI) was defined: the mean shear wave speed was computed on this ROI and the apparent shear modulus $\mu = \rho_0 v_s^2$ is deduced (with ρ_0 the density of the medium of interest, values of $1050 \text{ kg} \cdot \text{m}^{-3}$ and $1060 \text{ kg} \cdot \text{m}^{-3}$ were used for the TI PVA phantom (Fromageau *et al.*, 2007), and the *ex vivo* muscular tissues (Méndez and Keys, 1960), respectively. In this ROI, the standard deviation of the shear wave speed was used to compute the error on μ . At zero stress, μ_{\parallel} and μ_{\perp} were estimated depending on the configuration.

The relations between the measured apparent shear modulus μ and the applied stress σ are analyzed based on the previously derived AE theory in TI incompressible media. In each configuration and for each sample, the relation between μ and the applied stress σ is plotted. A least squares linear regression is used to fit experimental data and to retrieve the slopes γ_i , with i the configuration number (Fig. 1). The slopes γ_i enable to study the expected relations [Eq. (13)] between the AE equations and to estimate the NLSM A of each studied sample by using Eq. (14). The errors on the estimated parameters are derived using the error propagation formula based on the errors on the slopes (estimated from the linear regression), and on μ_{\parallel} and μ_{\perp} . Particularly, based on Eq. (14), the expression of the error on the NLSM A is as

follows (the Δ signs preceding A , μ_{\parallel} , μ_{\perp} , γ_1 , and γ_2 is used to refer to the error on the corresponding variable):

$$\Delta A = 4[\mu_{\perp}(\Delta\gamma_1 + \Delta\gamma_2) + \Delta\mu_{\parallel} + |\gamma_1 - \gamma_2|\Delta\mu_{\perp}] \quad (15)$$

IV. RESULTS

AE experiments on four muscular tissue samples and one TI PVA phantom are presented in this section. Data acquired at zero stress first allowed the assessment of the linear elastic characteristics of the TI samples. As an example, Figs. 3(A) and 3(B) show B-mode images acquired on the same muscular tissue sample, at zero stress, with the probe oriented parallel [Fig. 3(A)] and perpendicular [Fig. 3(B)] to the fibers. These images helped to validate the orientation of the probe with respect to the fiber axis for the rest of the experiment. In the PVA phantom, such fibers were naturally not visible, but the stretching direction guided the positioning of the probe. In such configurations, SWE measurements yield maps of the local shear wave speed v_s , on which the estimations of the linear shear moduli parallel μ_{\parallel} [Fig. 3(C)] and perpendicular μ_{\perp} [Fig. 3(D)] are based ($\mu_{\parallel,\perp} = \rho_0 v_{s(\parallel,\perp)}^2$) depending on the orientation of the probe. The shear wave speed values obtained in the configuration where the probe is parallel to the

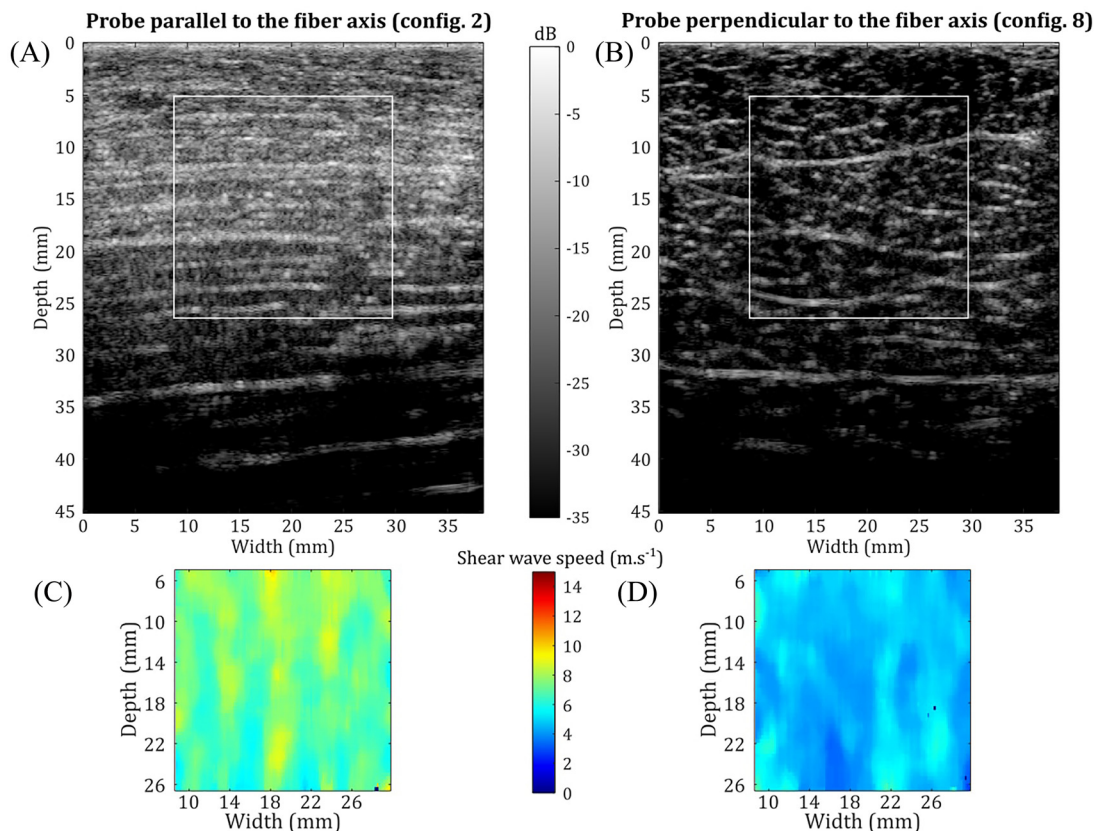


FIG. 3. (Color online) B-mode ultrasound images and local shear wave velocity maps of a bovine muscular tissue at zero stress for μ_{\parallel} and μ_{\perp} estimations. The four images in this figure have been acquired on the same bovine muscular tissue [referred to as the beef muscle (1) sample in Tables II and III] at zero stress. (A) and (B) B-mode ultrasound images obtained with the probe placed parallelly (A) or perpendicularly (B) to the fiber axis (configurations 2 and 8, respectively). (C) and (D) Local shear wave velocity maps measured using SSI on B-mode images (A) and (B), respectively. The white rectangles on (A) and (B) indicate the position of the shear wave speed measurement ROIs of (C) and (D), respectively.

TABLE III. Linear (μ_{\parallel} , μ_{\perp}) and nonlinear (A) elastic characterization of the investigated TI samples and validation of two theoretical relations (13) among the AE equations ($\gamma_1 - \gamma_4 = 0$ and $\gamma_7 - \gamma_8 = -1$).

Sample	TI-PVA	Beef muscle (1)	Beef muscle (2)	Pork muscle (3)	Pork muscle (4)
μ_{\parallel} (kPa)	29.5 ± 2.1	56.6 ± 13.1	54.3 ± 1.9	39.5 ± 4.6	23.9 ± 4.4
μ_{\perp} (kPa)	13.3 ± 0.7	26.6 ± 4.6	19.0 ± 2.4	22.7 ± 5.0	19.3 ± 2.9
A (kPa)	292.8 ± 146.5	-709.4 ± 931.7	677.1 ± 821.4	122.9 ± 649.1	391.8 ± 704.7
$\gamma_1 - \gamma_4$	0.6 ± 1.1			-1.9 ± 8.3	-3.6 ± 10.6
$\gamma_7 - \gamma_8$		-0.1 ± 4.8			0.6 ± 5.0

fiber axis [Fig. 3(C)] are globally higher than that for which the probe was placed perpendicular to the fibers [Fig. 3(D)]. The differences between the estimated shear moduli of a given sample (with μ up to twice as high as μ_{\perp} ; see Table III) demonstrate its anisotropic (TI) nature.

Note that shear wave speeds measured with the probe's axis in the direction of the medium's principal axis (configurations 4 to 6 at zero stress) were also used to estimate μ_{\parallel} .

Figure 4 depicts the evolution of the shear wave speed of one muscular tissue submitted to increasing uniaxial compression in configurations 2 and 8. These two configurations differ only in the propagation direction of the shear wave with respect to the fiber axis (parallel in configuration 2, perpendicular in configuration 8). In these two cases, the shear wave speed increases with stress and the evolution of the mean shear modulus over the studied ROI is represented on Fig. 5(B) (orange circles and purple squares for configurations 2 and 8, respectively). Nevertheless, the shear modulus evolution is different in the two configurations, as expected in the AE theory since the evolution depends on specific combinations of both the linear and NL elastic coefficients of the medium.

For configuration i measured on a given sample, μ_{\parallel} or μ_{\perp} (depending on the configuration number) is estimated at zero stress, and the slope γ_i is obtained through a least

squares linear regression of the apparent shear modulus versus stress.

AE experiment measurements were carried out independently on each sample and the evolutions of the apparent shear modulus as a function of stress are presented in Fig. 5 for the TI PVA phantom and for one muscular tissue. For each sample, as many configurations as possible were investigated, given its size and the stability of the system. Note that in the case of muscular tissues, configurations 4 to 6 were difficult to measure due to the low signal to noise ratio of the ultrasonic signal when the ultrasound axis is parallel to the fiber axis. Besides, configurations 3, 6, and 9 were not measured as the sample was not rigid enough to keep the fibers correctly oriented during the experiment. Indeed, configurations 3, 6, and 9 require the stress to be applied parallel to the fibers, meaning the fibers need to be oriented vertically. This would have resulted in irreproducible measurements not matching the three theoretical configurations at hand.

In each configuration and sample, the apparent shear modulus increases with stress (except for the TI PVA phantom in configuration 2). As expected in the AE theory, this evolution is linear with stress. Experimental data were fitted using a least squares linear regression (the estimated linear relation is represented on the plots with colored lines in

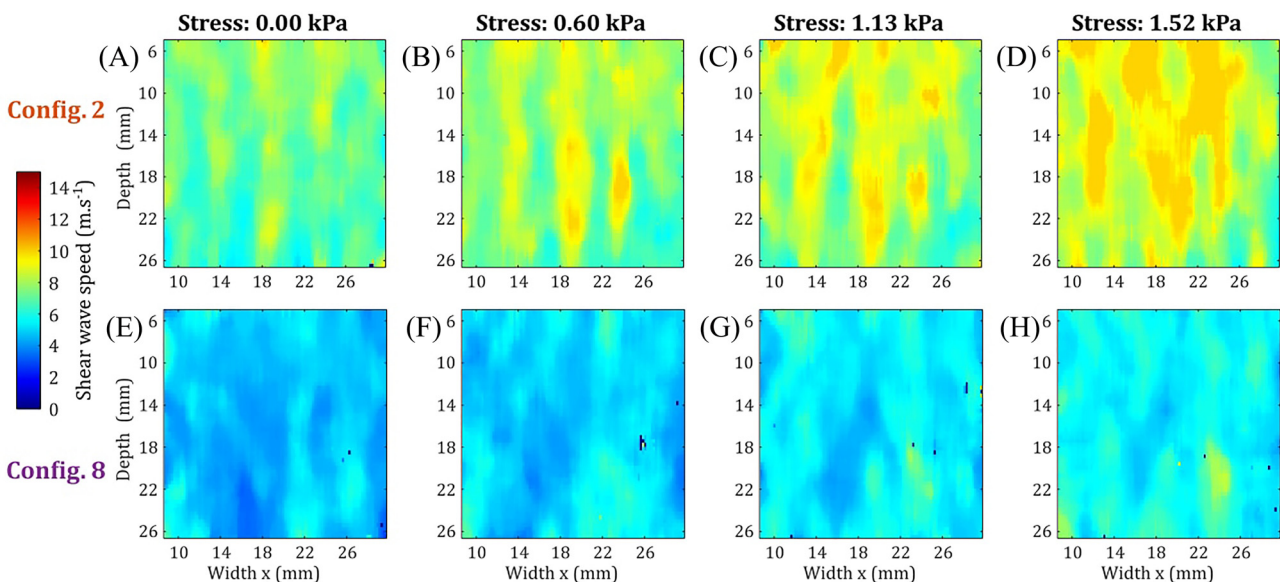


FIG. 4. (Color online) Evolution of the shear wave speed in a bovine muscular tissue under increasing uniaxial stress. (A-D, E-H) Local shear wave speed maps measured in configurations 2 and 8, respectively under 0, 0.60, 1.13, and 1.52 kPa uniaxial stresses oriented parallelly to the probe axis. All shear wave speed maps have been obtained on bovine muscular sample 1, for the two ROIs indicated on Fig. 3(A) (for A–D maps) and Fig. 3(B) (for E–H maps).

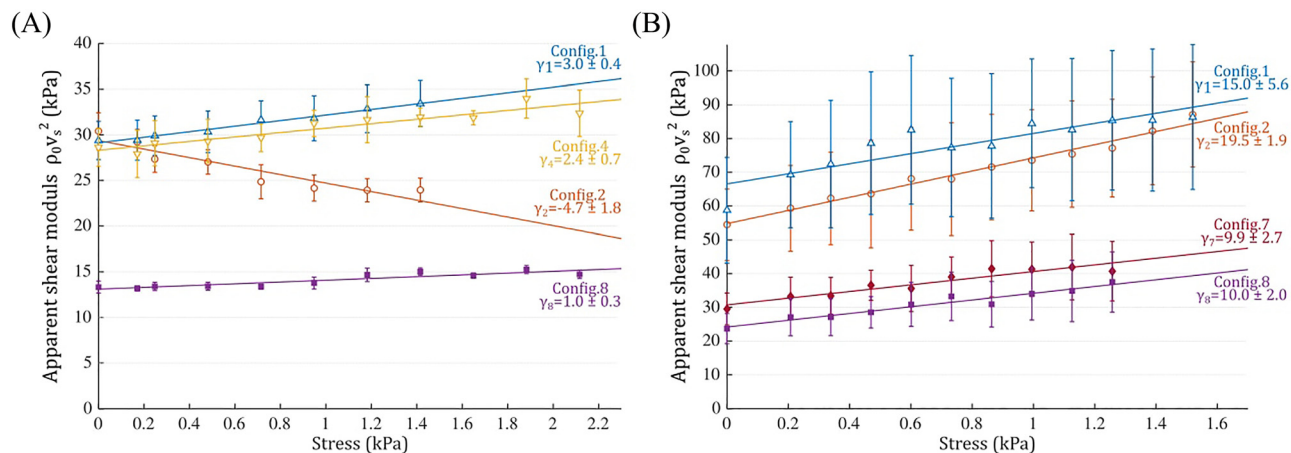


FIG. 5. (Color online) AE data sets acquired on two samples. Apparent shear modulus as a function of stress in each measured configuration in the TI PVA phantom (A) and in the bovine muscular sample #1 (B). Each color and marker shape correspond to a given configuration. The colored lines correspond to the linear relations between the apparent shear modulus and stress estimated through a least squares linear regression. The error on the apparent shear modulus is estimated based on the standard deviation of the local shear wave speed over the analyzed region of interest (ROI).

Fig. 5) to quantify the apparent shear modulus change with respect to stress. The values of the slopes shown in Table II for each sample vary from one sample to the other and from one configuration to the other (except between configurations 7–8 and 1–4). Note that the determination coefficients obtained from the linear regressions range from 0.769 to 0.981, confirming the $\rho v_s^2 - \sigma$ linear relations.

By using Eq. (14), the NLSM A of the investigated samples were estimated based on the values of the slopes of configurations 1 and 2, as well as on the measured shear moduli $\mu_{||}$ and μ_{\perp} (Table III). In *ex vivo* muscular tissues, A was of hundreds of kPa, either negative or positive. Note that when available, configuration 4 data could have been also used to retrieve A . However, since the quality of the SWE data is poorer in configuration 4 than in configuration 1, data from configuration 1 were preferred to that of configuration 4.

Finally, when data were available for one given sample, the relations [Eq. (13)] between equations related to different configurations were tested. Differences between the slopes related to configurations 1 and 4 on the one hand, and to configurations 7 and 8 on the other, were computed (Table III). For each sample and tested relation, the theory-based expected values [0 and -1 for (1)–(4) and (7)–(8), respectively) lay within the confidence interval of the computed differences.

V. DISCUSSION

In this work, the AE theory in TI incompressible media was successfully developed, making the investigation of the elastic NL of TI soft tissues, and more particularly of muscles, possible. Up to now, most NL elasticity studies were based on the AE theory previously developed for soft tissues under the reductive hypothesis of isotropy (Gennisson *et al.*, 2007). The adaptation of the AE theory to TI soft tissues required to consider the specificities of the TI geometry in terms of its second (linear) and 3rd order elastic properties. Using a different formalism, Destrade *et al.*

(2010) had already developed the AE theory for TI biological soft tissues submitted to a stress parallel to the fiber axis. They expressed the speed of shear waves as a function of the angle θ between the propagation direction of the wave and the fiber axis (the polarization and propagation directions of the wave form a plane containing the fiber axis). For specific values of θ matching with the previously defined configurations ($\theta = 0$ and $\frac{\pi}{2}$ corresponding to configurations 3 and 6 defined in Fig. 1, respectively), the two developments get to the same shear wave speed expressions. Compared to Destrade *et al.* (2010), our contribution here is to cover the cases where stress is perpendicular to the principal direction of the TI medium. Nevertheless, our development is restricted to the nine simplest configurations (Fig. 1), where the principal direction, stress, shear wave polarization and propagation are either parallel or perpendicular to each other.

To take advantage of the developed theory and verify it, AE experiments were carried out on two types of TI material: a TI PVA phantom and *ex vivo* muscular tissues. The relations predicted by the theory between different AE configurations were verified, and the first experimental measurements of the NLSM A of *ex vivo* biological TI tissues were successfully proposed. Note that Remenieras *et al.* (2021) recently characterized *in vivo* skeletal striated muscles using the AE theory in TI incompressible media. In particular, they quantified the slopes of the *flexor digiti minimi* muscle’s apparent shear modulus–stress relationships in configurations 3 and 9, by using the contraction of the muscle of interest as a source of stress. Nevertheless, since the NLSM A cannot be retrieved from the measurements of the slopes in these 2 configurations, it is difficult to compare their results with the estimations reported in this paper.

In all biological samples, the order of magnitude of the estimated NLSM A is of hundreds of kPa (in absolute value), which is approximately 10 times higher than the linear shear moduli $\mu_{||}$ and μ_{\perp} . The order of magnitude of our A estimations for muscular tissues is similar to that of

previous NLSM measurements in *ex vivo* isotropic tissues, such as bovine liver (Latorre-Ossa *et al.*, 2012; Bernal *et al.*, 2016). Experimentally, in the present paper and previous ones (Gennisson *et al.*, 2007; Latorre-Ossa *et al.*, 2012; Bernal *et al.*, 2016), a factor 10 is found between μ and A . This can be put into question since theoretically Destrade and Ogden (2010) showed that these two parameters are of the same order. Nevertheless, two quantities are of the same order of magnitude if their ratio is close or less to 10. Table III shows that this ratio varies from 3.1 to 16.4. Thus, we can assume that μ and A are of the same order, considering the experimental errors affecting the estimation of μ and A . Note that since the estimated NLSM A of TI incompressible media is related to only isotropic strain tensor invariants (independent from the principal direction) similarly to the isotropic NLSM A , this comparison is meaningful. However, the reported NLSM values in isotropic tissues are negative, while three of our estimations tend to be positive. Nevertheless, this needs to be considered cautiously given the size of the confidence intervals of our A estimations, which include negative values for each estimation. The difference in the nature of muscular and liver tissues can also explain discrepancies in their NL elastic characteristics.

From our estimations, the porcine or bovine origin of the muscular tissues seems to have little impact on the values of the NLSM, but more measurements are needed to confirm this assertion. However, the precision of the NLSM A estimation is very poor (the order of magnitude of the associated measurement uncertainties is similar to that of the estimated A values). This stems from the fact that the A estimation relies on the experimental measurements of four parameters ($\mu_{//}$, μ_{\perp} , and the slopes of configurations 1 and 2, γ_1 and γ_2), each associated with their error. Altogether, the amplitude of the resulting confidence interval related to A is high. Nevertheless, among the different terms in the expression of the error on A [Eq. (15)], the first term which involves the errors on the γ_1 and γ_2 slopes dominates others. Therefore, the improvement of γ_1 and γ_2 estimations would reduce the experimental error associated with A .

Furthermore, due to the highlighted dependence between the nine AE equations [Eq. (13)] giving six relations among the nine equations, A is the only NLSM that can be estimated out of the three NLSM present in the AE equations, even if all configurations were experimentally accessible. Indeed, the linear elastic parameter $E_{//}$ adds up to the three unknown NLSM, making the system (i.e., the nine slope value expressions) undetermined. To access the values of H and K based on AE, $E_{//}$ must be therefore measured beforehand independently. Due to the TI nature of the media, $E_{//}$ is independent from $\mu_{//}$ and μ_{\perp} and cannot be deduced from simple SWE measurements (Royer *et al.*, 2011), unlike in isotropic incompressible media for which the Young modulus E is usually estimated based on the shear modulus μ_0 using $E \approx 3\mu_0$. In the magnetic resonance (MR) elastography field, a measure of $E_{//}$ was proposed by Guo *et al.* (2016) based on the full shear wave field measurement and its inversion. In the ultrasound field, however,

the measure of $E_{//}$ is delicate and not yet fully developed. Recent work based on the variations of the velocity of SV (shear vertical) mode waves with respect to the polarization direction managed to put forward the first estimations of $E_{//}$ by using SWE (Knight *et al.*, 2020; Li *et al.*, 2016a; Li *et al.*, 2016b). But the experimental application of this method is challenging in terms of precision and its implementation on all muscles is not simple. To retrieve $E_{//}$, another possible strategy would be to experimentally measure the ratios of lateral and axial static strains when the TI medium is submitted to a stress perpendicular to the principal direction axis. (These ratios can be shown to depend upon $E_{//}$, $\mu_{//}$, and μ_{\perp}). Nevertheless, lateral strain estimations remain a major challenge (Lopata *et al.*, 2009).

We were faced with several experimental difficulties, challenging our data. First of all, the investigated muscular tissues were not perfectly homogeneous, as it can be seen on shear wave speed maps [Figs. 3(C) and 3(D)] at the submillimetric scale, but also at the scale of the entire tissue. This can explain the discrepancies between the estimations of $\mu_{//}$ and μ_{\perp} from different configurations [Fig. 5(B); Table II], since the probes were necessarily placed at different positions on the muscular tissue to match with the different configurations. Moreover, since the estimation of A relies on measurements from at least three different configurations, and so from at least three different positions, the accuracy of our A estimation can be impacted by the heterogeneity of the medium.

Second, the simplifying hypotheses defining the configurations (Fig. 1) for which the AE equations were developed in this paper, were difficult to verify experimentally. The positioning of the muscle sample with its principal axis aligned or not with the probe axis or the stress axis was operator dependent. In the future, AE experiments in TI media may benefit from methods, such as Backscatter Tensor Imaging (BTI) (Papadacci *et al.*, 2014), for more precise detection of fiber orientation. Nevertheless, positioning the muscle tissue sample such that the uniaxial stress is rigorously perpendicular or parallel to the fibers will remain an issue.

Finally, there was an experimental trade-off between the size of the sample, to measure as many configurations as possible (particularly this was an issue when the probe was to be oriented vertically), and the evenness of the upper surface of the sample, on which relied the homogeneity of the applied stress. Therefore, in some configurations, the estimation of the applied stress might not be perfectly accurate, affecting the values of the slopes obtained from linear regressions of $\rho_0 v_s^2$ with respect to stress (Fig. 5).

All in all, this work on the AE theory in TI incompressible media proposes a first and new approach for the estimation of the NLSM A of muscles. The method in and of itself remains difficult to implement due to the experimental constraints to respect to match the defined configurations. Indeed, the latter imply that the principal direction of the TI medium, the ultrasound probe axis and the stress axis have to be either parallel or perpendicular to one another. Further development (more tedious but using the same reasoning) is needed to include the angle dependency of stress and of the

shear plane to remove these constraints. Besides, a future perspective, even more challenging but no less substantial, is to translate such measurements in *in vivo* muscles. In addition to the aforementioned challenges, this would imply developing a setup enabling the application of uniaxial, homogeneous, and quantifiable stress on *in vivo* muscles. Depending on the investigated muscle, a specific setup would have to be developed, to apply a uniaxial stress *in vivo*. Similarly, a specific algorithm would be needed to track fiber orientation. Nevertheless, such measurements would contribute to bringing insight on the NL elastic behavior of muscles and might provide physicians with new clinical biomarkers. Furthermore, by linearly relating the apparent shear modulus to local stress, this theoretical work proposes a possible framework for the estimation of local stress in muscles.

ACKNOWLEDGMENT

This work was partly funded by the ANR INNOVAN (Grant No. ANR-19-CE19-0017) and France Life Imaging (Grant No. ANR-11-INBS-0006). The authors would like to gratefully thank Stefan Catheline, Bruno Giammarinaro, Jean-Pierre Remenieras, and Xavier Jacob for scientific and helpful discussions, as well as Laurène Jourdain and Simon Chatelin for their support in the realization of the experimental setup and phantoms.

Bercoff, J., Tanter, M., and Fink, M. (2004). "Supersonic shear imaging: A new technique for soft tissue elasticity mapping," *IEEE Trans. Ultrason. Ferroelect. Freq. Contr.* **51**, 396–409.

Bernal, M., Chamming's, F., Couade, M., Bercoff, J., Tanter, M., and Gennisson, J.-L. (2016). "In vivo quantification of the nonlinear shear modulus in breast lesions: Feasibility study," *IEEE Trans. Ultrason. Ferroelect. Freq. Contr.* **63**, 101–109.

Bower, A. F. (2010). *Applied Mechanics of Solids* (Boca Raton, FL), pp. 794.

Brillouin, L. (1925). "Les tensions de radiation; leur interprétation en mécanique classique et en relativité," ("The tensions of radiation and their interpretation in terms of classical mechanics and relativity)," *J. Phys. Radium* **6**(11), 337–353.

Chadwick, P. (1993). "Wave propagation in incompressible transversely isotropic elastic media I. Homogeneous plane waves," *Proc. R. Ir. Acad.* **93**(A), 231–253.

Chatelin, S., Bernal, M., Defieux, T., Papadacci, C., Flaud, P., Nahas, A., Boccara, C., Gennisson, J.-L., Tanter, M., and Pernot, M. (2014). "Anisotropic polyvinyl alcohol hydrogel phantom for shear wave elastography in fibrous biological soft tissue: A multimodality characterization," *Phys. Med. Biol.* **59**, 6923–6940.

Destrade, M., Gilchrist, M. D., and Ogden, R. W. (2010). "Third- and fourth-order elasticities of biological soft tissues," *J. Acoust. Soc. Am.* **127**, 2103–2106.

Destrade, M., and Ogden, R. W. (2010). "On the third- and fourth-order constants of incompressible isotropic elasticity," *J. Acoust. Soc. Am.* **128**, 3334–3343.

Fromageau, J., Gennisson, J.-L., Schmitt, C., Maurice, R. L., Mongrain, R., and Cloutier, G. (2007). "Estimation of polyvinyl alcohol cryogel mechanical properties with four ultrasound elastography methods and comparison with gold standard testings," *IEEE Trans. Ultrason. Ferroelect. Freq. Contr.* **54**, 498–509.

Gennisson, J.-L., Rénier, M., Catheline, S., Barrière, C., Bercoff, J., Tanter, M., and Fink, M. (2007). "Acoustoelasticity in soft solids: Assessment of the nonlinear shear modulus with the acoustic radiation force," *J. Acoust. Soc. Am.* **122**, 3211–3219.

Gennisson, J.-L., Defieux, T., Macé, E., Montaldo, G., Fink, M., and Tanter, M. (2010). "Viscoelastic and anisotropic mechanical properties of *in vivo* muscle tissue assessed by Supersonic Shear Imaging," *Ultrasound Med. Biol.* **36**(5), 789–801.

Guo, J., Hirsch, S., Scheel, M., Braun, J., and Sack, I. (2016). "Three-parameter shear wave inversion in MR elastography of incompressible transverse isotropic media: Application to *in vivo* lower leg muscles," *Magn. Reson. Med.* **75**, 1537–1545.

Hamilton, M. F., Ilinskii, Y. A., and Zabolotskaya, E. A. (2004). "Separation of compressibility and shear deformation in the elastic energy density (L)," *J. Acoust. Soc. Am.* **116**, 41–44.

Hayes, M., and Rivlin, R. S. (1961). "Surface waves in deformed elastic materials," *Arch. Ration. Mech.* **8**, 358–380.

Hughes, D. S., and Kelly, J. L. (1953). "Second-order elastic deformation of solids," *Phys. Rev.* **92**, 1145–1149.

Johnson, G. C. (1982). "Acoustoelastic response of polycrystalline aggregates exhibiting transverse isotropy," *J. Nondestruct. Eval.* **3**, 1–8.

Knight, A. E., Trutna, C. A., Rouze, N. C., Hobson-Webb, L. D., Palmeri, M. L., Caenen, A., and Nightingale, K. R. (2020). "Demonstration of complex shear wave patterns in skeletal muscle *in vivo* using 3D SWEI," in *2020 IEEE International Ultrasonics Symposium (IUS)*, pp. 1–4.

Landau, L. D., Pitaevskii, L. P., Kosevich, A. M., and Lifshitz, E. M. (1985). *Theory of Elasticity*, 3rd ed. (Butterworth-Heinemann, Oxford), pp. 195.

Latorre-Ossa, H., Gennisson, J.-L., De Brosses, E., and Tanter, M. (2012). "Quantitative imaging of nonlinear shear modulus by combining static elastography and shear wave elastography," *IEEE Trans. Ultrason. Ferroelect. Freq. Contr.* **59**, 833–839.

Li, G.-Y., Zheng, Y., Liu, Y., Destrade, M., and Cao, Y. (2016a). "Elastic Cherenkov effects in transversely isotropic soft materials-I: Theoretical analysis, simulations and inverse method," *J. Mech. Phys. Solids* **96**, 388–410.

Li, G.-Y., He, Q., Qian, L.-X., Geng, H., Liu, Y., Yang, X.-Y., Luo, J., and Cao, Y. (2016b). "Elastic Cherenkov effects in transversely isotropic soft materials- II: Ex vivo and *in vivo* experiments," *J. Mech. Phys. Solids* **94**, 181–190.

Lopata, R. G. P., Nillesen, M. M., Hansen, H. H. G., Gerrits, I. H., Thijssen, J. M., and de Korte, C. L. (2009). "Performance evaluation of methods for two-dimensional displacement and strain estimation using ultrasound radio frequency data," *Ultrasound Med. Biol.* **35**, 796–812.

Méndez, J., and Keys, A. (1960). "Density and composition of mammalian muscle," *Metabolism* **9**, 184–188.

Namani, R., Feng, Y., Okamoto, R. J., Jesuraj, N., Sakiyama-Elbert, S. E., Genin, G. M., and Bayly, P. V. (2012). "Elastic characterization of transversely isotropic soft materials by dynamic shear and asymmetric indentation," *J. Biomed. Eng.* **134**, 061004.

Ogden, R. W. (1984). *Non-Linear Elastic Deformations* (Dover Publications, Great Britain), pp. 562.

Papadacci, C., Tanter, M., Pernot, M., and Fink, M. (2014). "Ultrasound backscatter tensor imaging (BTI): Analysis of the spatial coherence of ultrasonic speckle in anisotropic soft tissues," *IEEE Trans. Ultrason. Ferroelect. Freq. Contr.* **61**, 986–996.

Remenieras, J.-P., Bulot, M., Gennisson, J.-L., Patat, F., Destrade, M., and Bacle, G. (2021). "Acousto-elasticity of transversely isotropic incompressible soft tissues: Characterization of skeletal striated muscle," *Phys. Med. Biol.* **66**, 145009.

Rosen, D., and Jiang, J. (2019). "Analyzing acoustoelastic effect of shear wave elastography data for perfused and hydrated soft tissues using a macromolecular network inspired model," *J. Biomech.* **97**, 109370.

Royer, D., Gennisson, J.-L., Defieux, T., and Tanter, M. (2011). "On the elasticity of transverse isotropic soft tissues (L)," *J. Acoust. Soc. Am.* **129**, 2757–2760.

Spencer, A. J. M. (Ed.) (1984). *Continuum Theory of the Mechanics of Fibre-Reinforced Composites* (Springer Vienna, Vienna).